Localization of a sound source in uniform horizontal linear motion using a pair of acoustic sensors

Kam W. Lo

Defence Science & Technology Group, Maritime Division, 13 Garden Street, Eveleigh, NSW 2015, Australia

ABSTRACT

Acoustic sensors can be used to localize moving sound sources. The trajectory of a sound source moving in air or under water at constant velocity along a horizontal linear path is fully specified by a set of five motion parameters. The first part of this paper describes a motion parameter estimation method for a broadband source in transit using inter-sensor multipath delay measurements from a pair of acoustic sensors located in the same medium (air or water) as the source. The performances of the method in the air and underwater domains are evaluated using real data recorded, respectively, from a ground-based microphone array in a field experiment for ten different transits of a jet aircraft, and from a bottom-mounted hydrophone array in a shallow water experiment for four different transits of a small vessel and a single transit of a rigid-hulled inflatable boat. The second part of this paper describes a motion parameter estimation method for a transiting broadband airborne source that contains a narrowband component using both instantaneous frequency and time delay measurements from a pair of underwater acoustic sensors. The performance of the method is evaluated using real data recorded from a towed hydrophone array in a deep water experiment for four different transits of a turbo-prop aircraft.

1 INTRODUCTION

Acoustic sensors can be used to localize moving sound sources (Sedunov, Sutin, Salloum, and Sedunov 2015, Lo and Ferguson 2012). The trajectory of a sound source moving in air or under water at constant velocity along a horizontal linear path is fully specified by a set of five motion parameters: velocity, altitude or depth, time of closest point of approach (CPA) to a sensor, horizontal range at CPA, and azimuth angle at CPA (Lo and Ferguson 2001). Therefore, the localization or tracking problem is reduced to a source motion parameter estimation problem. A single ground-based acoustic sensor (microphone) is only able to estimate some of the motion parameters of an airborne source including its speed, CPA time, and CPA slant range or altitude (Ferguson and Quinn 1994, Lo, Ferguson, Gao, and Maguer 2003). To estimate the entire set of the source motion parameters requires an array of sensors. Traditionally a wide-aperture acoustic array is used. For narrowband sources, instantaneous frequency (IF) measurements from the array are processed (Lo and Ferguson 2001), while for broadband sources, time delay (TD) measurements from the array are processed (Ferguson and Lo 2000). Recently, two techniques have been proposed to improve the precision of the source motion parameter estimates for a small aperture array (Lo 2013, Lo 2016). The first technique, which is applicable to broadband sources, utilizes inter-sensor multipath delay (MD) measurements from the array (Lo 2013). Using this technique, it was shown that a three-element array with a 0.9-m inter-sensor spacing is able to provide precise estimates of all five motion parameters of a broadband airborne source in transit (Lo 2013). The second technique, which is applicable to broadband sources that contain a narrowband component, utilizes both IF and TD measurements (instead of only TD measurements) from a three-element planar array (Lo 2016). It was shown that the technique greatly improves the precision of the source velocity and altitude estimates for a three-element L-shaped array with a 0.9-m inter-sensor spacing (Lo 2016). This paper considers estimating the entire set of motion parameters of a moving sound source in transit using only a pair of acoustic sensors. It is assumed that the left-right ambiguity can be resolved by some means or it is known *a priori* on which side (left or right) of the array the source's CPA position is located. The first part of this paper describes the source motion parameter estimation method using inter-sensor MD measurements from a pair of acoustic sensors located in the same medium as the source (first technique). Its performance is evaluated first in the air domain using real data recorded from a ground-based microphone array in a field experiment for ten different transits of a jet aircraft, and then in the underwater domain using real data recorded from a bottom-mounted hydrophone array in a shallow water experiment for four different transits of a small vessel and a single transit of a rigid-hulled inflatable boat (RHIB). In the second part of the paper, the source motion parameter estimation method using both IF and TD measurements from a pair of acoustic sensors located in the same medium as the source (second technique) is extend-

ed to the case where the two sensors are located in a medium different from the source. The performance of the method is evaluated using real data recorded from a towed hydrophone array in a deep water experiment for four different transits of a turbo-prop aircraft.

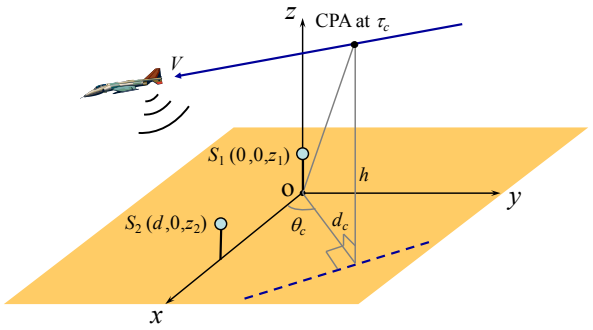

Figure 1: Geometric configuration for a pair of sensors and the linear trajectory of an acoustic source in transit. The sensors are located in the same medium as the source.

2 MOTION PARAMETER ESTIMATION USING INTER-SENSOR MULTIPATH DELAY MEASUREMENTS

2.1 Method (air domain)

Figure 1 shows a pair of acoustic sensors located above the *xy*-plane (ground) and the linear trajectory of an airborne source as it transits past the sensor pair at constant velocity V and constant altitude h. The positions of sensor 1 (denoted as S_1) and sensor 2 (denoted as S_2) are given respectively by $(0,0,z_1)$ and $(d,0,z_2)$. The source position at any time τ is given by

$$x(\tau) = d_c \cos\theta_c + (\tau - \tau_c)V \sin\theta_c\,,\ y(\tau) = d_c \sin\theta_c - (\tau - \tau_c)V \cos\theta_c\,,\ z(\tau) = h, \tag{1}$$

where τ_c is the time of CPA to S_1 (or the origin *O*), d_c is the horizontal range at CPA, and θ_c is the azimuth angle at CPA $(-\pi < \theta_c \leq \pi)$. The source velocity V is either positive or negative, depending on whether the origin *O* is on the source's right- or left-hand side as the source moves along its trajectory. Also, the source speed $|V|$ is assumed to be subsonic, i.e., $|V| < c_a$, where c_a is the (iso)speed of sound in air. The source trajectory is completely specified by the five motion parameters $\{V, \tau_c, h, d_c, \theta_c\}$.

The source emits continuously a broadband acoustic signal, which arrives at each sensor via a direct path and a multipath (ground-reflected path). If the speed of the source is not much less than the speed of sound, the source will have moved to a very different position by the time its emitted signal arrives at any one of the two sensors, and this so-called "retardation effect" must be taken into account when formulating the source motion parameter estimation algorithm. The signal emitted by the source at time τ arrives at S_m via the direct path at time $t_m^d = \tau + R_m^d(\tau)/c_a$, where $R_m^d(\tau)$ is the length of the direct path from the source to S_m at time τ, for $m = 1,2$. The same signal arrives at S_m via the multipath at time $t_m^r = \tau + R_m^r(\tau)/c_a$, where $R_m^r(\tau)$ is the length of the multipath from the source to S_m at time τ, for $m = 1,2$. Let $D_{21}^{dd}(t)$ denote the differential time of arrival (DTOA) between the direct path signal at S_2 and the direct path signal at S_1 at time t, $D_{21}^{rd}(t)$ the DTOA between the multipath signal at S_2 and the direct path signal at S_1 at time t , and $D_{21}^{dr}(t)$ the DTOA between the direct path signal at S_2 and the multipath signal at S_1 at time t. By definition, at time $t = t_1^d$,

$$D_{21}^{\alpha\beta}(t) \triangleq t_2^{\alpha} - t_1^{\beta} = [R_2^{\alpha}(\tau) - R_1^{\beta}(\tau)]/c_a, \quad \text{for } \alpha\beta = dd, rd \text{ and } dr. \tag{2}$$

The DTOA $D_{21}^{dd}(t)$ is referred to as TD, while $D_{21}^{\alpha\beta}(t)$ is referred to as inter-sensor MD for $\alpha \neq \beta$. Each of these three DTOAs varies with time t as the source position changes with time τ. Time t denotes signal receiving time at S_1 (or sensor time), whereas τ denotes signal emission time (or source time). At any given time t, the DTOA between the direct path/multipath signal at S_1 and the direct path/multipath signal at S_2 can be estimated by first performing a short-time cross-correlation of the outputs of the two sensors and then finding the time lag corre-

sponding to the appropriate peak of the cross-correlation function. In this case, the cross-correlation function is dominated by a strong peak [corresponding to $D_{21}^{dd}(t)$] and two weaker peaks [corresponding to $D_{21}^{rd}(t)$ and $D_{21}^{dr}(t)$]. Using the sensor coordinates and (1), it can be shown that

$$R_m^d(\tau) = \{V^2(\tau-\tau_c)^2 + d_c^2 + (h-z_m)^2 - 2x_m[d_c\cos\theta_c + (\tau-\tau_c)V\sin\theta_c] + x_m^2\}^{1/2}, \quad (3)$$

$$R_m^r(\tau) = \{V^2(\tau-\tau_c)^2 + d_c^2 + (h+z_m)^2 - 2x_m[d_c\cos\theta_c + (\tau-\tau_c)V\sin\theta_c] + x_m^2\}^{1/2}, \quad (4)$$

where x_m is the *x*-coordinate of S_m, for $m = 1,2$. Substituting the expression for $R_1^d(\tau)$ and $t = t_1^d$ into $t_1^d = \tau + R_1^d(\tau)/c_a$, and then solving the resulting quadratic equation for τ gives

$$\tau = \tau_c + \frac{c_a^2(t-\tau_c) - \left[R_c^2(c_a^2-V^2) + V^2c_a^2(t-\tau_c)^2\right]^{1/2}}{(c_a^2-V^2)}, \quad (5)$$

where $R_c = [d_c^2 + (h-z_1)^2]^{1/2}$ is the slant range of the source from S_1 at CPA. Equations (2)–(5) constitute a delay model (which predicts the variations with sensor time t of the TD and inter-sensor MDs) for S_1 and S_2. Define the source motion parameter vector $\boldsymbol{\lambda} = [V, \tau_c, h, d_c, \theta_c]^T$, where the superscript *T* denote vector transpose. This delay model is a function of time t and $\boldsymbol{\lambda}$, i.e., $D_{21}^{\alpha\beta}(t) \equiv D_{21}^{\alpha\beta}(t, \boldsymbol{\lambda})$ for $\alpha\beta = dd, rd$ and dr.

Let $\hat{D}_{21}^{\alpha\beta}(t)$ be the estimate of $D_{21}^{\alpha\beta}(t)$. The nonlinear least-squares estimate (NLS) of $\boldsymbol{\lambda}$ is given by

$$\hat{\boldsymbol{\lambda}} = \arg\min_{\boldsymbol{\lambda}'} \sum_{n=1}^{N} \| \hat{\mathbf{f}}(t_n) - \mathbf{f}(t_n, \boldsymbol{\lambda}') \|^2, \quad (6)$$

where $\boldsymbol{\lambda}' = [V', \tau_c', h', d_c', \theta_c']^T$, $\hat{\boldsymbol{\lambda}} = [\hat{V}, \hat{\tau}_c, \hat{h}, \hat{d}_c, \hat{\theta}_c]^T$, $\hat{\mathbf{f}}(t_n) = [\,\hat{D}_{21}^{dd}(t_n),\ \hat{D}_{21}^{rd}(t_n),\ \hat{D}_{21}^{dr}(t_n)\,]^T$ and $\mathbf{f}(t_n, \boldsymbol{\lambda}') = [D_{21}^{dd}(t_n, \boldsymbol{\lambda}'), D_{21}^{rd}(t_n, \boldsymbol{\lambda}'), D_{21}^{dr}(t_n, \boldsymbol{\lambda}')]^T$ are the observation and model vectors at time t_n $(1 \le n \le N)$, respectively, and $\|\cdot\|$ denotes l_2 norm of a vector. It is assumed that the observation time interval $(t_1,\ t_N)$ is sufficiently long that it covers both inbound and outbound legs of the source transit. The minimization (6) is subject to the following constraints:

$$[\mathrm{sgn}(V) - 1]c/2 < V' < [\mathrm{sgn}(V) + 1]c/2,\ \ \hat{\tau}_c^0 - \Delta\tau_{\max} < \tau_c' < \hat{\tau}_c^0 - \Delta\tau_{\max},$$

$$0 < h' < h_{\max},\ \ 0 < d_c' < d_{c,\max},\ \ [\mathrm{sgn}(\theta_c) - 1]\pi/2 < \theta_c' < [\mathrm{sgn}(\theta_c) + 1]\pi/2, \quad (7)$$

where $\hat{\tau}_c^0$ is the initial estimate of τ_c, $\Delta\tau_{\max}$ is the maximum possible error in $\hat{\tau}_c^0$, $h_{\max}$ and $d_{c,\max}$ are the maximum altitude and CPA horizontal range, respectively, and $\mathrm{sgn}(\cdot)$ denotes the sign of the quantity in brackets. In this paper, the left-right ambiguity is resolved by assuming *a priori* knowledge of $\mathrm{sgn}(\theta_c)$. The sign of V is determined using the TD measurements: when $\theta_c > 0$, $V < 0$ if $\hat{D}_{21}^{dd}(t_N) > \hat{D}_{21}^{dd}(t_1)$, and $V > 0$ otherwise; whereas, when $\theta_c < 0$, $V < 0$ if $\hat{D}_{21}^{dd}(t_N) < \hat{D}_{21}^{dd}(t_1)$, and $V > 0$ otherwise. The initial estimate $\hat{\tau}_c^0$ is obtained by finding the time when the received signal energy at S_1 attains its maximum.

2.2 Experimental results (air domain)

A 21-element planar microphone array was used in a field experiment (Lo 2013). All 21 sensors, labelled M_1 to M_{21}, were located at a height of 0.55 m above a level ground (*xy*-plane) composed of compact soil. Fifteen of the sensors, M_1 to M_{15}, were uniformly spaced at 0.9 m on a straight line parallel to and directly over the *x*-axis. The output of each sensor was sampling at a frequency of 7111 Hz. Acoustic data were recorded for 10 transits of a jet aircraft travelling at a nominal speed of 154 m/s. The aircraft's nominal altitudes were 305 m for transits 1 and 2, 381 m for transits 3 and 4, 457 m for transits 5 and 6, 533 m for transits 7 and 8, and 610 m for transits 9 and 10. The flight path of the aircraft during each transit was level with the ground and approximately parallel to the *x*-axis. The speed of sound in air was 340 m/s. Sensors M_1 to M_{14} were used to form 13 sensor pairs, each consisting of two adjacent sensors. For a given sensor pair, data from each sensor were processed in overlapping blocks, each containing 2048 samples, with 50% overlap between two consecutive data blocks. Each data block of the first sensor was cross-correlated with the corresponding data block of the second sensor. The cross-correlation processing was implemented in the frequency domain using the fast Fourier transform, with a rectangular spectral window from 50 to 3555 Hz. For each sensor pair, the first three peaks of the cross-

correlation function were refined using three-point quadratic interpolation, and the locations of the refined peaks provided the TD and inter-sensor MD estimates. In this way, a series of TD estimates and two series of inter-sensor MD estimates were obtained for each sensor pair. Figure 2(a) shows the normalized cross-correlogram (an intensity plot showing the normalized cross-correlation function as a function of time) of the 13rd sensor pair for aircraft transit 10. In this example, $\{S_1, S_2\} = \{M_{14}, M_{13}\}$. Three time-lag tracks were observed, with the upper, middle, and lower tracks representing $\widehat{D}_{21}^{rd}(t)$, $\widehat{D}_{21}^{dd}(t)$, and $\widehat{D}_{21}^{dr}(t)$, respectively. Figure 2(b) shows, as black circles, these three time series of estimates and, as red lines, the least-squares (LS) fit of the delay model to these estimates.

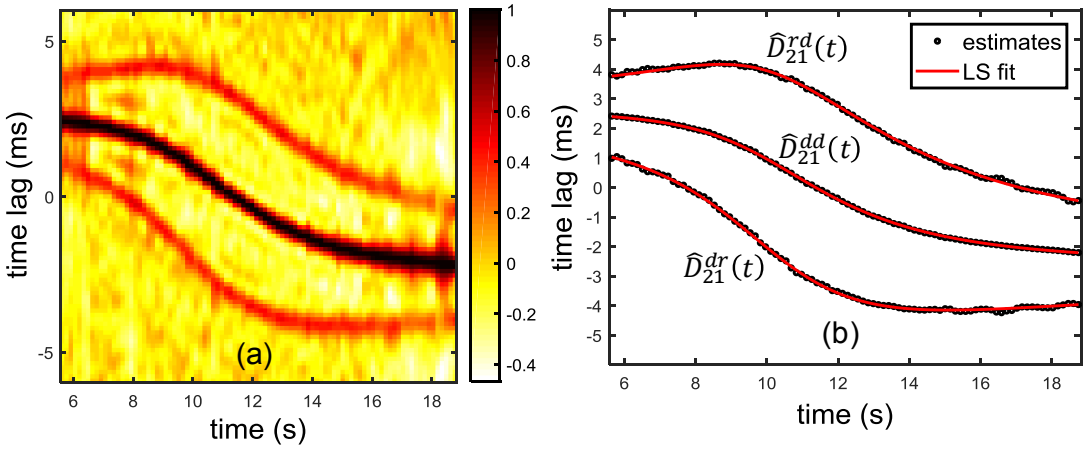

Figure 2: (a) Normalized cross-correlogram of sensor pair $\{M_{14}, M_{13}\}$ for aircraft transit 10. (b) Corresponding times series of TD and inter-sensor MD estimates (black circles) and LS fit of delay model (red lines).

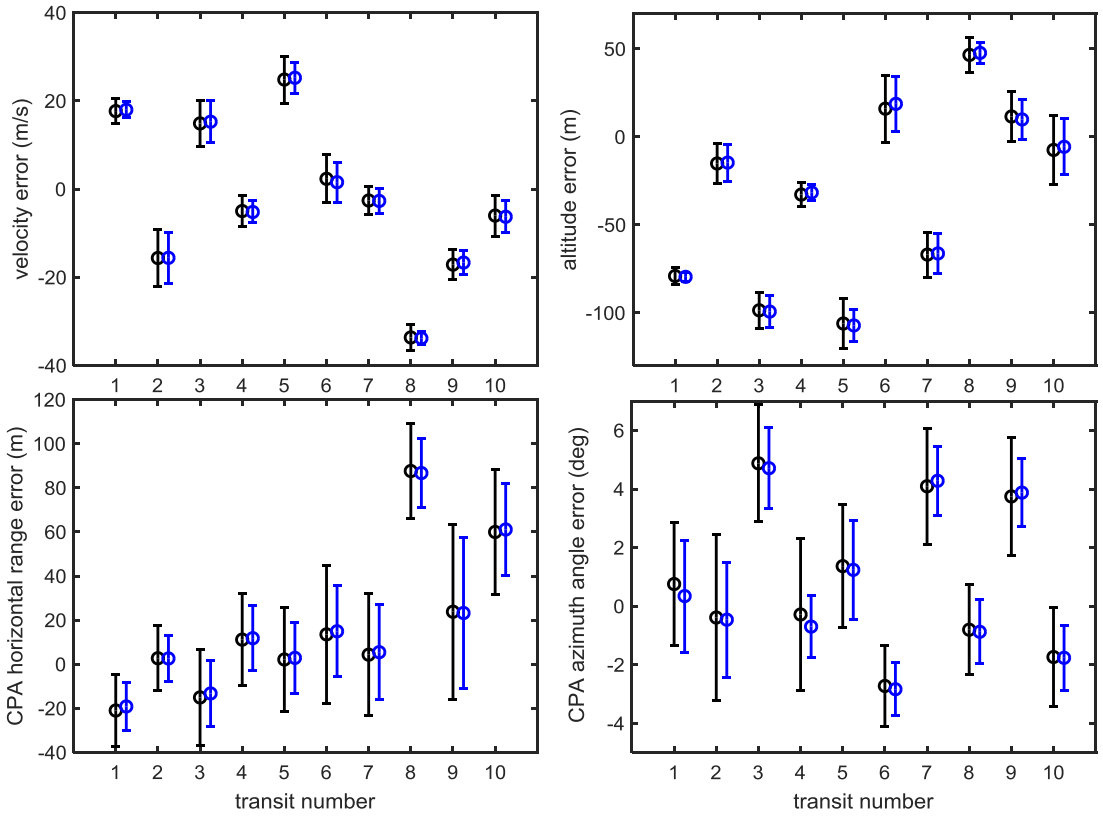

Figure 3: Bias errors (circles) and ±1 standard deviation (error bars) in the estimates of $\{V, h, d_c, \theta_c\}$ for the 10 jet aircraft transits. Results are shown in black for using 2 sensors and in blue for using 3 sensors.

A different local *xy*-coordinate system was set up for each sensor pair such that the local *x*-coordinate of its first sensor was always zero. The source motion parameter estimation method was applied in turn to each of the 13 sensor pairs. The minimization (6) was implemented in MATLAB® using the global optimization solver *GlobalSearch* in conjunction with the minimization algorithm *fmincon*. The initial estimates of $|V|$ and h were assigned typical values of 75 m/s and 200 m, respectively, and the initial estimates of d_c and θ_c were simply set to zero. Also, $\Delta\tau_{\max} = 10$ s, and $h_{\max} = d_{c,\max} = 1$ km in (7). The statistics of the 13 sets of motion parameter estimates $\{\hat{V}, \hat{\tau}_c, \hat{h}, \hat{d}_c, \hat{\theta}_c\}$, one set per sensor pair, were compiled (after correcting the estimates of τ_c and d_c from each sensor pair using the method described in a previous paper (Lo 2013) so that the corrected values all refer to the CPA to M_{19}) for each aircraft transit. Figure 3 shows the bias errors and ±1 standard deviation in the estimates of $\{V, h, d_c, \theta_c\}$ for each of the 10 aircraft transits. The bias errors were computed by subtracting the nominal values from the mean values. The nominal values of d_c (at CPA to M_{19}) and θ_c were assumed to be 60 m and ±90°, respectively, for each transit. Also included in Fig. 3 for comparison purposes are the results obtained with two sensor pairs formed by three consecutive microphones (Lo 2013), instead of a single sensor pair. As it is uncertain how close the nominal values are to the actual values, it is the precision (or variability), rather than the bias errors, of the motion parameter estimates that is of interest here. The average standard deviations in the estimates of $\{V, \tau_c, h, d_c, \theta_c\}$ over all 10 transits are 4.3 m/s, 0.05 s, 12.3 m, 24.6 m, and 2.0°, respectively, when using two sensors, and 3.4 m/s, 0.04 s, 9.6 m, 18.0 m, and 1.3°, respectively, when using three sensors. Using an additional sensor provides slightly better results.

2.3 Method (underwater domain)

The method can be used to estimate the motion parameters of a broadband underwater (or surface) source using a pair of hydrophones located above the sea bottom. In this case, the *xy*-plane coincides with the sea bottom, h represents the height of the source above the sea bottom, and c_a is replaced by c_w, the (iso)speed of sound in water. Also, as $c_w \gg |V|$, the "retardation effect" can be ignored, i.e., $R_1^\beta(\tau) \cong R_1^\beta(t)$ and $R_2^\alpha(\tau) \cong R_2^\alpha(t)$, for $\alpha\beta = dd, rd$ and dr. Therefore, (2) reduces to

$$D_{21}^{\alpha\beta}(t) = [R_2^\alpha(t) - R_1^\beta(t)]/c_w, \quad \text{for } \alpha\beta = dd, rd \text{ and } dr. \tag{8}$$

There are a lot of multipaths in an underwater environment. The bottom-reflected path may not be used (because its associated inter-sensor MD tracks are unresolvable from the TD track in the correlogram). The correct multipath needs to be identified by some means before the motion parameter estimation method can be applied. For a surface source, the bottom-surface-reflected path is often used and therefore (4) is replaced by

$$R_m^r(t) = \{V^2(t-\tau_c)^2 + d_c^2 + (h - z_m + 2w)^2 - 2x_m[d_c \cos\theta_c + (t-\tau_c)V \sin\theta_c] + x_m^2\}^{1/2}, \tag{9}$$

where w is the water depth and z_m is now the height of sensor *m* above the sea bottom. In this case, the cross-correlation function for S_1 and S_2 is dominated by a strong positive peak [corresponding to $D_{21}^{dd}(t)$] and two weaker negative peaks [corresponding to $D_{21}^{rd}(t)$ and $D_{21}^{dr}(t)$].

2.4 Experimental results (underwater domain)

An eight-element linear hydrophone array was used in a shallow water experiment (Lo and Ferguson 2014a). The water depth is 21.5 m. The eight sensors, labelled H_1 to H_8, were located at a height of 1 m above the sea floor, with an inter-sensor spacing of 14 m. The output of each sensor was sampled at a frequency of 250 kHz. Acoustic data were recorded for four different transits of a small vessel (transits 1 to 4) travelling at a nominal speed of 4.6 m/s and a single transit of a RHIB (transit 5) travelling at a nominal speed of 10.8 m/s. The trajectory of the small vessel was approximately perpendicular to the array axis, while the trajectory of the RHIB is inclined at approximately 25° to the array axis. The nominal values of d_c (at CPA to H_4) for transits 1 to 5 are 130, 135, 89, 83, and 25 m, respectively. The speed of sound in water was 1520 m/s. Owing to data acquisition/time synchronization problems among some hydrophones, only four sensor pairs were formed: $\{S_1, S_2\} = \{H_3, H_4\}$, $\{H_5, H_6\}$, $\{H_6, H_7\}$, and $\{H_7, H_8\}$. The data processing was similar to that for the microphones, except now that (1) each data block contained 65,536 samples, (2) the phase transform prefiltering technique was used to suppress ambiguous peaks which would otherwise have appeared in the cross-correlation function due to the strong harmonic components of the source signal, and (3) the spectral window was from 50 to 1000 Hz. Figure 4 shows (a) the normalized cross-correlogram and (b) the time series of TD and inter-sensor MD estimates (denoted by black circles) for the second sensor pair $\{H_5, H_6\}$ for the fourth small vessel transit. Also shown in Fig. 4(b) is the

LS fit of the delay model (denoted by red lines) to the TD and inter-sensor MD estimates. Figure 5 shows the corresponding results for the RHIB transit. The source motion parameter estimation method was applied in turn to each of the four sensor pairs. The initial estimates of $|V|$ and d_c were assigned typical values of 5 m/s and 50 m, respectively, and the initial estimate θ_c was simply set to zero. The water depth w was used as an initial estimate of h. Also, $\Delta\tau_{\max} = 10$ s, $h_{\max} = w$, and $d_{c,\max} = 500$ m in (7). The statistics of the four sets of motion parameter estimates $\{\hat{V}, \hat{\tau}_c, \hat{h}, \hat{d}_c, \hat{\theta}_c\}$, one set per sensor pair, were compiled (after correcting the estimates of τ_c and d_c from each sensor pair so that the corrected values all refer to CPA to H_4) for each small vessel or RHIB transit. Figure 6 shows the bias errors and ±1 standard deviation in the estimates of $\{V, h, d_c, \theta_c\}$ for each of the five transits. The average standard deviations in the estimates of $\{V, \tau_c, h, d_c, \theta_c\}$ over all five transits are 0.09 m/s, 0.34 s, 0.51 m, 1.82 m, and 0.85°, respectively.

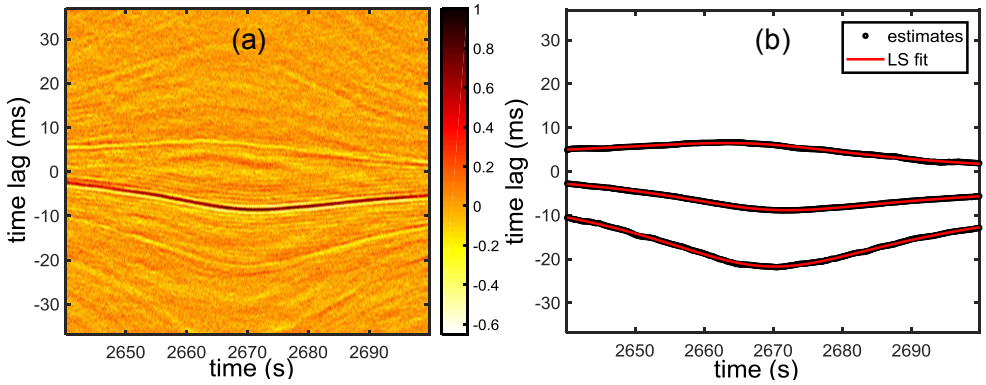

Figure 4: (a) Normalized cross-correlograms of sensor pair $\{H_5, H_6\}$ for vessel transit 4. (b) Corresponding time series of TD and inter-sensor MD estimates (black circles) and LS fit of delay model (red lines).

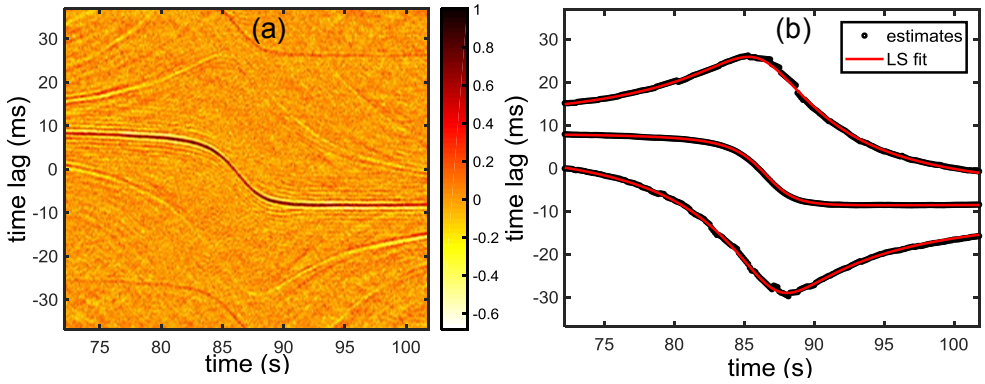

Figure 5: (a) Normalized cross-correlograms of sensor pair $\{H_5, H_6\}$ for the RHIB transit. (b) Corresponding time series of TD and inter-sensor MD estimates (black circles) and LS fit of delay model (red lines).

3 MOTION PARAMETER ESTIMATION USING IF AND TIME DELAY MEASUREMENTS

3.1 Method (airborne source and underwater sensors)

The propagation of sound from an airborne source to a pair of hydrophones under water is modelled by applying the geometric ray theory to the two isospeed media (air and sea) separated by the planar air-sea interface which coincides with the *xy*-plane. The positions of sensor 1 (S_1) and sensor 2 (S_2) are given respectively by $(0, 0, -d_1)$ and $(d, 0, -d_2)$, where d_1 and d_2 are the respective depths of S_1 and S_2 below the sea surface. The position of the source at any time τ is given by (1), where h is now the source altitude above the sea surface. Figure 7 shows the ray path from the source to S_m for $m = 1,2$. The signal emitted by the source at time τ arrives at S_m at a later time t given by

$$t = \tau + l_{am}(\tau)/c_a + l_{wm}(\tau)/c_w, \tag{10}$$

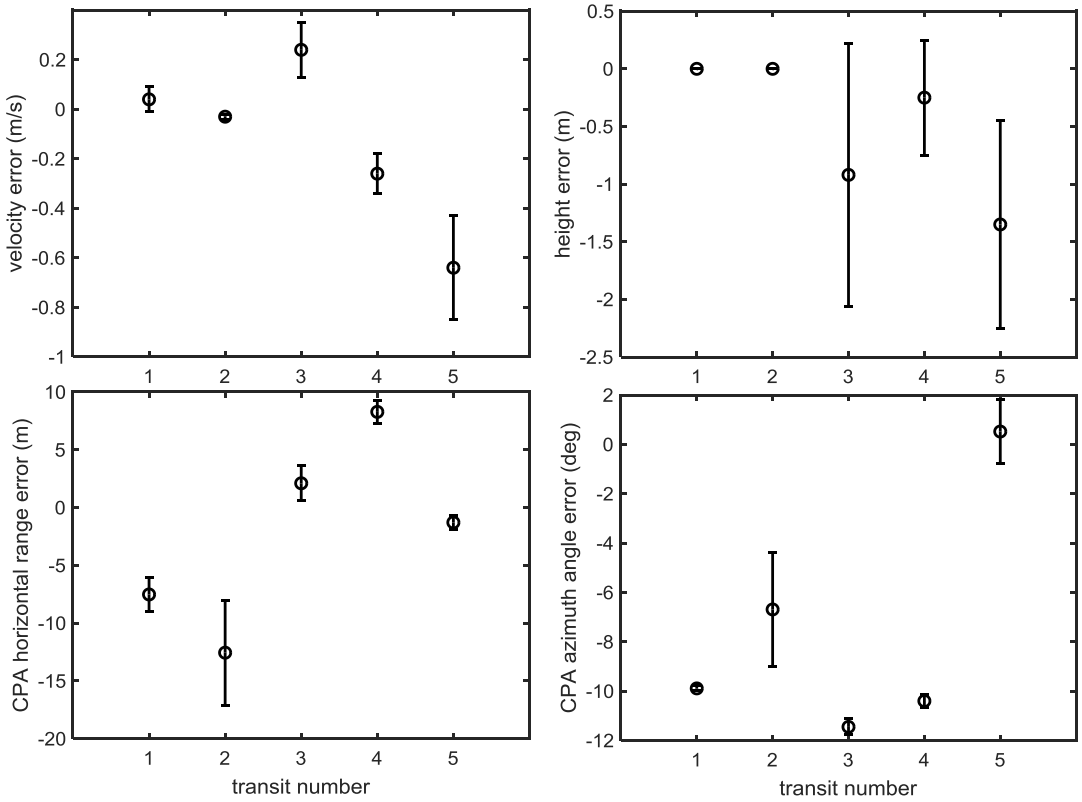

Figure 6: Bias errors (circles) and ± 1 standard deviation (error bars) in the estimates of $\{V, h, d_c, \theta_c\}$ for the four small vessel transits (transits 1 to 4) and the RHIB transit (transit 5).

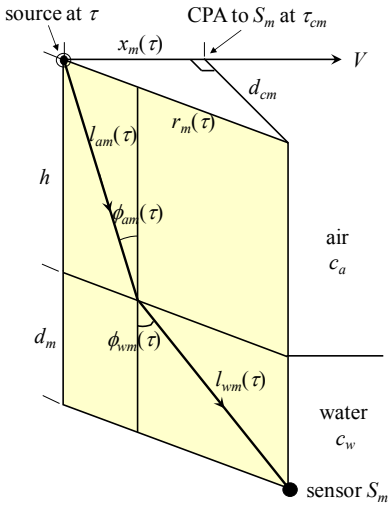

Figure 7: Ray path of sound emitted by a source in air at time τ arriving later at a sensor S_m under water.

where $l_{am}(\tau)$ and $l_{wm}(\tau)$ are the lengths of the ray paths in the air and sea media, respectively. An explicit expression for the signal emission time τ in terms of the signal receiving time t at sensor S_m has been derived elsewhere (Lo and Ferguson 2014b):

$$\tau = \tau_{cm} + \frac{c_w^2(t-\tilde{\tau}_{cm}) - [\tilde{h}_m^2(c_w^2 - V^2) + V^2 c_w^2 (t-\tilde{\tau}_{cm})^2]^{1/2}}{c_w^2 - V^2}, \tag{11}$$

where τ_{cm} is the time when the source is at CPA to S_m, $\tilde{\tau}_{cm} = \tau_{cm} + (1-\gamma^2)h/c_a$, and $\tilde{h}_m = \gamma h + l_{wmc}$, with $l_{wmc} = l_{wm}(\tau_{cm})$ and $\gamma = c_a/c_w$. The source emits continuously a broadband acoustic signal with a narrowband tone of constant frequency f_o. It has been shown that the IF of the narrowband tone received by S_m at time t is given by (Lo and Ferguson 2014b)

$$f_m(t) = f_o\left[1 + \frac{V^2(\tau-\tau_{cm})\sin\phi_{wm}(\tau)}{c_w r_m(\tau)}\right]^{-1}, \tag{12}$$

where $\phi_{wm}(\tau)$ is the angle of refraction (see Fig. 7), and $r_m(\tau) = [d_{cm}^2 + V^2(\tau-\tau_{cm})^2]^{1/2}$ is the horizontal range of the source from S_m at time τ, with $d_{cm} = r_m(\tau_{cm})$. By definition, $\tau_{c1} = \tau_c$ and $d_{c1} = d_c$. It can be shown that (Lo and Ferguson 2014b)

$$d_{c2} = |d_c - d\cos\theta_c\,|, \qquad \tau_{c2} = d\sin\theta_c/V + \tau_c. \tag{13}$$

Equations (11)–(13) constitute an IF model for the two sensors S_1 and S_2. This IF model is a function of time t, f_o, and $\boldsymbol{\lambda}$, i.e., $f_m(t) \equiv f_m(t, f_o, \boldsymbol{\lambda})$ for $m = 1, 2$. The methods to compute l_{wmc} in (11) and $\sin\phi_{wm}(\tau)$ in (12) can be found in a previous paper (Lo and Ferguson 2014b).

The signal receiving time t at S_1 is related to its emission time τ via (10) with $m = 1$. Given t, τ can be computed using (11) with $m = 1$. This value of τ can then be used in (10) with $m = 2$ to calculate the receiving time of the same signal at S_2. Subtracting the signal receiving time at S_1 from that at S_2 gives the DTOA (or TD) of the signal at the two sensors at time t:

$$D_{21}(t) = [l_{a2}(\tau) - l_{a1}(\tau)]/c_a + [l_{w2}(\tau) - l_{w1}(\tau)]/c_w. \tag{14}$$

From Fig. 7, $l_{am}(\tau) = h/\cos\phi_{am}(\tau)$ and $l_{wm}(\tau) = d_m/\cos\phi_{wm}(\tau)$. Both equations can be expressed in terms of $\sin\phi_{wm}(\tau)$ instead of $\cos\phi_{am}(\tau)$ or $\cos\phi_{wm}(\tau)$ by using the identity $\cos\theta = \sqrt{1-\sin^2\theta}$ and Snell's law: $\sin\phi_{am}(\tau)/c_a = \sin\phi_{wm}(\tau)/c_w$. Therefore, $D_{21}(t)$ is readily computed once $\sin\phi_{wm}(\tau)$ is calculated. Equations (11) and (14) constitute a TD model for the two sensors S_1 and S_2. This TD model is a function of time t and $\boldsymbol{\lambda}$, i.e., $D_{21}(t) \equiv D_{21}(t, \boldsymbol{\lambda})$.

The NLS estimates of $\{f_o, \boldsymbol{\lambda}\}$ are given by

$$\{\hat{f}_o, \hat{\boldsymbol{\lambda}}\} = \arg\min_{f_o', \boldsymbol{\lambda}'} \sum_{m=1}^{2}\sigma_{f_m}^{-2}\sum_{n=1}^{N_{fm}}|\hat{f}_m(t_{f_m,n}) - f_m(t_{f_m,n}, f_o, \boldsymbol{\lambda}')|^2 + \sigma_D^{-2}\sum_{n=1}^{N_D}|\hat{D}_{21}(t_{D,n}) - D_{21}(t_{D,n}, \boldsymbol{\lambda}')|^2, \tag{15}$$

where $\hat{f}_m(t_{f_m,n})$ is the IF measurement from S_m at time $t_{f_m,n}$, for $1 \le n \le N_{f_m}$ and $m = 1, 2$; $\hat{D}_{21}(t_{D,n})$ is the TD measurement from the sensor pair at time $t_{D,n}$, for $1 \le n \le N_D$; $\sigma_{f_m}^2$ is the error variance in the IF measurements from S_m and σ_D^2 is the error variance in the TD measurements from the sensor pair. The minimization (15) is subject to the set of constraints given in (7) and an additional constraint: $0 < f_o' < f_{o,\max}$. In this paper, the left-right ambiguity is resolved by assuming *a priori* knowledge of $\mathrm{sgn}(\theta_c)$. The initial estimate of d_c is set to a small value, here 5 m. The methods to obtain the initial estimates of $f_o, |V|, \tau_c$, and h can be found in a previous paper (Lo and Ferguson 2014b). Let $|\hat{V}|^0$, $\hat{\tau}_c^0$, $\hat{h}^0$, and $\hat{d}_c^0$ denote the initial estimates of $|V|, \tau_c, h$, and d_c, respectively. To determine the sign of V and obtain an initial estimate of θ_c, the second summation term in (15) is evaluated at $\boldsymbol{\lambda}' = [|\hat{V}|^0, \hat{\tau}_c^0, \hat{h}^0, \hat{d}_c^0, \theta_c']^{\boldsymbol{T}}$ and $[-|\hat{V}|^0, \hat{\tau}_c^0, \hat{h}^0, \hat{d}_c^0, \theta_c']^{\boldsymbol{T}}$ for a discrete set of values of θ_c' ranging from its lower bound to its upper bound at increments of 9^o. The set of values, either $\{|\hat{V}|^0, \hat{\theta}_c^0\}$ or $\{-|\hat{V}|^0, \hat{\theta}_c^0\}$, that result in the smallest value of the summation term provide the initial estimates of $\{V, \theta_c\}$.

Since $\sigma_{f_m}^2$ and σ_D^2 are unknown, a two-step procedure is proposed to compute their estimates, along with $\{\hat{f}_o, \hat{\boldsymbol{\lambda}}\}$.
(1) Assign a typical value of 1 Hz to σ_{f_m} and a typical value of 1 ms to σ_D, and compute $\{\hat{f}_o, \hat{\boldsymbol{\lambda}}\}$ using (15).
(2) Estimate $\sigma_{f_m}^2$ as the variance of the residues $\hat{f}_m(t_{f_m,n}) - f_m(t_{f_m,n}, \hat{f}_o, \hat{\boldsymbol{\lambda}}), 1 \le n \le N_{f_m}$, and σ_D^2 as the variance of the residues $\hat{D}_{21}(t_{D,n}) - D_{21}(t_{D,n}, \hat{\boldsymbol{\lambda}}), 1 \le n \le N_D$. Then use these values of $\sigma_{f_m}^2$ and σ_D^2 in (15) to recompute $\{\hat{f}_o, \hat{\boldsymbol{\lambda}}\}$.

3.2 Experimental results (airborne source and underwater sensors)

A 24-element linear towed hydrophone array was used in a deep sea experiment (Ferguson and Lo 1999). The water depth was 4500 m. The 24 hydrophones, labelled H_1 to H_{24}, were uniformly spaced at 7.5 m and located 18 m below the sea surface. The speeds of sound were 340 m/s in air and 1524 m/s in water (between the sea surface and the sensors). The output of each sensor was sampled at a frequency of 5333 Hz. Acoustic data were recorded for several transits of a turbo-prop aircraft. Four of these aircraft transits are considered in this paper. The flight path of the aircraft was approximately directly over and along the axis of the linear array for each transit. The aircraft's nominal velocities and altitudes for transits 1 to 4 were (123 m/s, 151 m), (125 m/s, 305 m), (122 m/s, 610 m), and (-119 m/s, 1843 m), respectively. The propeller blade rate of the aircraft (corresponding to the source frequency f_o) was 68 Hz, independent of its velocity. The acoustic data had been processed in previous work (Ferguson and Lo 1999) which resulted in a time series of IF estimates for each sensor and time series of TD estimates for several sensor pairs with various inter-sensor spacings, for each of the four aircraft transits. Four of these sensor pairs: $\{H_{11,}H_9\}$, $\{H_{12,}H_{10}\}$, $\{H_{13,}H_{11}\}$, and $\{H_{14,}H_{12}\}$ have an inter-sensor spacing of 15 m. Figure 8 shows, as circles, (a) the two time series of IF estimates and (b) the time series of TD estimates for sensor pair $\{H_{14,}H_{12}\}$ for aircraft transit 2. Also shown, as black lines, in Fig. 8 is the LS fit of the IF and TD models simultaneously to the IF and TD estimates. The source motion parameter estimation method was applied in turn to each of the four sensor pairs. It was assumed that the actual flight path was displaced (if any) to the left-hand side of the array axis, i.e., $0 \le \theta_c \le \pi$. Also, $\Delta\tau_{\max} = 10$ s, $h_{\max} = 5$ km, $d_{c,\max} = 100$ m, and $f_{o,\max} = 1$ kHz. The results for all four sensor pairs were used to compute the statistics of the source parameter estimates. Figure 9 shows the bias errors and ± 1 standard deviation in the estimates of $\{V, h, d_c, \theta_c\}$ for each aircraft transit. The average standard deviations in the estimates of $\{V, \tau_c, h, d_c, \theta_c\}$ over all four transits are 3.3 m/s, 0.18 s, 58.4 m, 9.6 m, and 3.9°, respectively. The average root-mean-square error in the estimates of f_o over all four transits is 0.17 Hz.

4 CONCLUSIONS

Two methods for estimating the entire set of motion parameters of a sound source in uniform horizontal linear motion using a pair of acoustic sensors have been described. The first method, which is applicable to airborne or underwater broadband sources, utilizes inter-sensor MD measurements from the sensor pair located in the same medium (air or water) as the source. The second method, which is applicable to airborne broadband sources with a narrowband component, utilizes both IF and TD measurements from the sensor pair located under water. The total observation time interval for each of the two methods is required to be sufficiently long so that it covers both inbound and outbound legs of the source transit. Both methods have been tested using real data. The precision or variability of the source motion parameter estimates is satisfactory for both methods. Bias errors have been observed in the source motion parameter estimates, which are small in some cases and large in other cases. The observed bias errors are likely due to uncertainties in the nominal parameter values and the use of a simple, linear propagation model for sound in the source parameter estimation methods. Future research includes reformulating the source motion parameter estimation methods using a more realistic sound propagation model and reassessing their performances.

ACKNOWLEDGEMENT

The author would like to thank his colleague, Dr. Brian Ferguson, for providing the real data used in this paper.

REFERENCES

Sedunov, A., Sutin, A., Salloum, H., and Sedunov, N. 2015. 'Passive acoustic localization of small aircraft'. In Proceedings of Meetings on Acoustics 20: 055005.

Lo, K.W. and Ferguson, B.G. 2012. 'Diver Detection and Localization Using Passive Sonar'. In Proceedings of Acoustics 2012. Fremantle, Australia.

Lo, K.W. and Ferguson, B.G. 2001. 'Flight path estimation using frequency measurements from a wide aperture acoustic array'. IEEE Transactions on Aerospace and Electronic Systems 37: 685-694.

Ferguson, B.G. and Quinn, B.G. 1994. 'Application of the short-time Fourier transform and the Wigner-Ville distribution to the acoustic localization of aircraft'. Journal of Acoustical Society of America 96: 821-827.

Lo, K.W., Ferguson, B.G., Gao, Y., and Maguer, A. 2003. 'Aircraft flight parameter estimation using acoustic multipath delays'. IEEE Transactions on Aerospace and Electronic Systems 39: 259-268.

Ferguson, B.G. and Lo, K.W. 2000. 'Turboprop and rotary-wing aircraft flight parameter estimation using both narrow-band and broadband passive acoustic signal-processing methods'. Journal of Acoustical Society of America 108: 1763-1771.

Lo, K.W. 2013. 'Flight parameter estimation using time delay and intersensor multipath delay measurements from a small aperture acoustic array'. Journal of Acoustical Society of America 134: 17-28.
Lo, K.W. 2016. 'Flight parameter estimation using instantaneous frequency and time delay measurements from a three-element planar acoustic array'. Journal of Acoustical Society of America 139: 2386-2398.
Lo, K.W. and Ferguson, B.G. 2014a. 'Source motion parameter estimation using direct and multipath arrivals at a pair of hydrophones'. In Proceedings of 2nd International Conference and Exhibition on Underwater Acoustics, 775-782.
Lo, K.W. and Ferguson, B.G. 2014b. 'Flight parameter estimation using instantaneous frequency measurements from a wide aperture hydrophone array'. IEEE Journal of Oceanic Engineering 39: 607-619.
Ferguson, B.G. and Lo, K.W. 1999. 'Transiting aircraft parameter estimation using underwater acoustic sensor data'. IEEE Journal of Oceanic Engineering 24: 424-435.

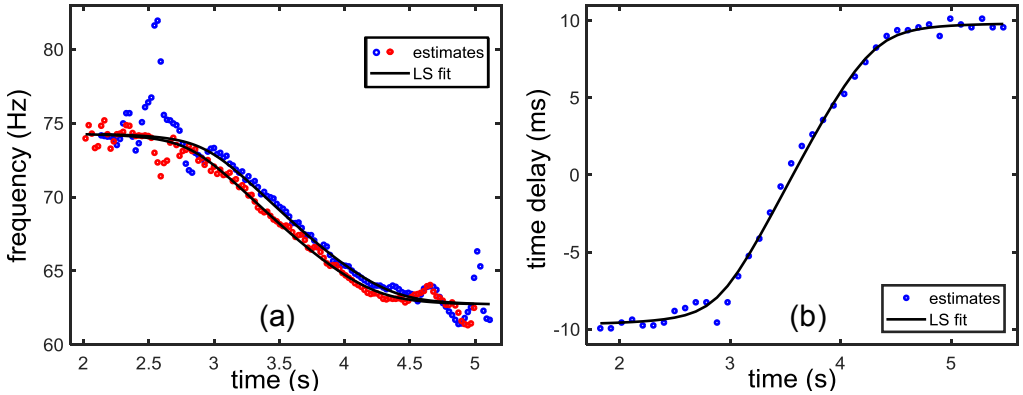

Figure 8: Time series of (a) IF estimates (red and blue circles) and (b) TD estimates (blue circles) and simultaneous LS fit of IF and TD models (black lines) for sensor pair $\{H_{14}, H_{12}\}$ for turboprop aircraft transit 2.

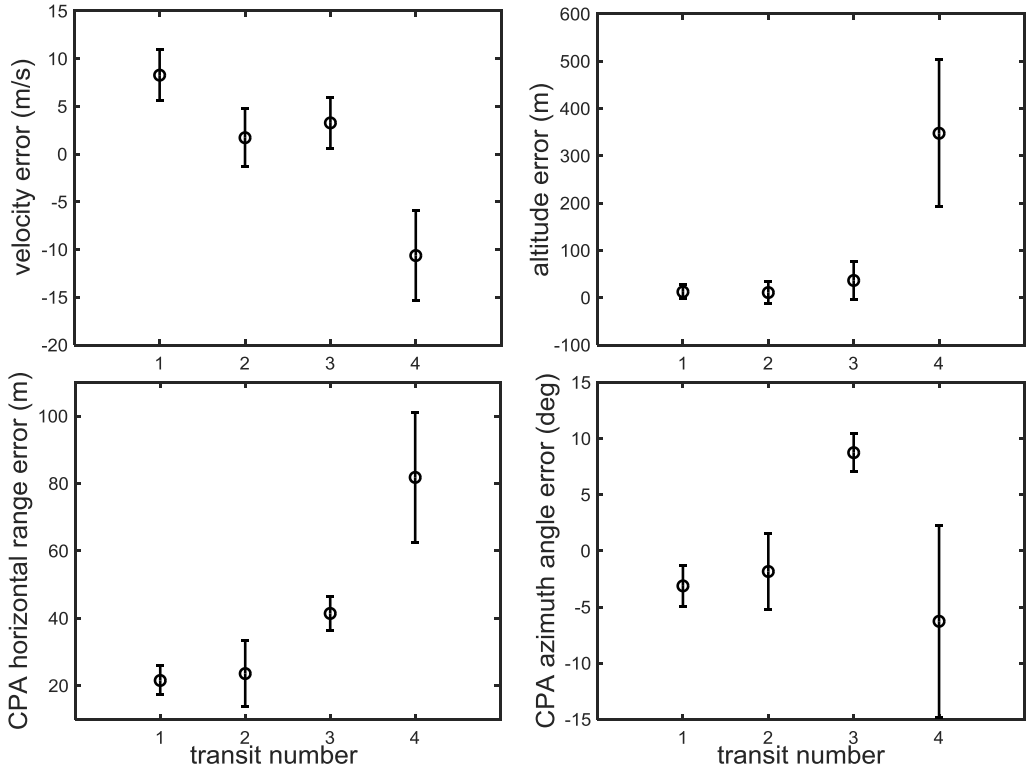

Figure 9: Bias errors (circles) and ±1 standard deviation (error bars) in the estimates of $\{V, h, d_c, \theta_c\}$ for the four turboprop aircraft transits.